Random Phase Approximation Spin - Isospin Nuclear Response In The Deep Inelastic Region.

(Article begins on next page)

16 August 2024

Random phase approximation spin-isospin nuclear response in the deep inelastic region

W. M. Alberico and A. Molinari
Istituto di Fisica Teorica dell'Università di Torino, 10125 Torino, Italy
and Istituto Nazionale di Fisica Nucleare, Sezione di Torino, Torino, Italy

A. De Pace
Institut für Theoretische Physik, Universitat Tubingen, D-7400 Tubingen, Federal Republic of Germany
and Istituto Nazionale di Fisica Nucleare, Sezione di Torino, Torino, Italy

M. Ericson
Université C. Bernard Lyon I, 69621 Villeurbanne, France
and European Organization for Nuclear Research, Geneva, Switzerland

Mikkel B. Johnson
Los Alamos National Laboratories, LAMPF, Los Alamos, New Mexico 87545
(Received 5 December 1985)

The spin-isospin volume responses of a finite nucleus are evaluated in the random phase approximation framework, utilizing a harmonic oscillator basis. Particular emphasis is given to the mixing between the longitudinal $(\sigma \cdot q)$ and transverse $(\sigma \times q)$ couplings, which arise at the nuclear surface. We show that it reduces somewhat the contrast between the two spin responses. We compare the calculated transverse response with the experimental one extracted from deep inelastic electron scattering.

I. INTRODUCTION

The nuclear spin-isospin response has been actively investigated, both experimentally and theoretically, in the past few years.[1,2] Accurate data[3] in the transverse channel have been provided by the inclusive (e,e') experiments in a number of light and medium nuclei over a large range of momentum transfers. Remarkably, in the region of the quasielastic peak, a universal behavior of the transverse response per particle, with a shape resembling the one of a Fermi gas, emerges from the experiment. One can thus conjecture that the latter can be reasonably accounted for in a nuclear matter framework.

Indeed, theoretical descriptions based on infinite nuclear matter either directly[4,5] or indirectly, as in semiclassical approaches,[6] have been rather successful in accounting for the data.

These studies point to the existence, at finite momentum transfer, of spin-isospin collective effects, the remnant, in the transverse channel, of the Gamow-Teller resonance. In the spin longitudinal channel, on the other hand, collective effects, if present, would be of particular significance, being a precursor of pion condensation.

In spite of these achievements, it appears worthwhile to explore the spin-isospin response in a finite nucleus, both to attain a deeper understanding of the reasons underlying the success of the nuclear matter approach and to elucidate the role of the nuclear surface in the process.

The influence of the latter is essentially twofold: Indeed, the surface lowers the density felt by the peripheral nucleons, thus hampering the development of a collective behavior. Moreover, the variation in space of the nuclear density leads, on one hand, to an additional suppression of collective effects, as was already shown to occur in the static situations;[7] on the other, it induces a coupling between the $(\sigma \cdot q)$ and $(\sigma \times q)$ vertices, which attenuates the predicted[4] contrast between the two spin responses. These effects are obviously enhanced when the probe mainly explores the *surface* of the nucleus, as does occur to some extent in the (p,p') inclusive scattering, particularly at large incident proton energies (≥ 0.5 GeV).

The surface spin-isospin response has already been calculated by Esbensen et al.[8] in a semi-infinite nuclear matter framework. We shall treat the surface response of a finite nucleus separately in a forthcoming paper;[9] here we will restrict ourselves to the volume responses, as probed, e.g., in the (e,e') scattering.

In this connection finite nuclei random phase approximation (RPA) calculations have already been performed, for both the responses and the wave functions, including the exchange contribution, a proper treatment of the continuum and the effects associated with the finite range of the force.[10–16] However, the Hilbert basis employed in these calculations is generally too narrow to allow a treatment of the response in the deep inelastic region at large momentum transfers. One exception is represented by the continuum RPA evaluation of Cavinato et al.[16] of the spin transverse response in ^{12}C, which utilizes a Skyrme interaction.

In the present paper we aim at solving the RPA equations for the generalized polarization propagator $\Pi_{\mu\nu}(q,q';\omega)$ (Ref. 17) (whose imaginary part is often referred to as response function) in a finite nucleus and in a basis large enough to allow an appropriate handling of the

spin-isospin response over a wide kinematical domain. This aim is, of course, best achieved by dealing directly with the response function rather than through a specific calculation of the RPA wave functions.

Yet the difficulties of the problem are such that we have simplified it by omitting both the exchange contribution and the description of the nuclear continuum. In fact, our basis, while being very large, is still a harmonic oscillator one. Concerning the exchange contribution, we hope to account for it, at least partially, by a convenient choice of the Landau-Migdal parameter g', the zero-range component of our interaction (the finite range ones being carried by the pion and the rho, as customary in the $\sigma\tau$ channel). Furthermore, the RPA integral equations for $\Pi_{\mu\nu}(\mathbf{q},\mathbf{q}';\omega)$, presented in Ref. 17, have been solved here along the lines of the approximation originally suggested by Toki and Weise[18] (hereafter referred to as TW), partly to avoid the heavy numeric required for an exact solution and partly because this method leads to analytic formulae which transparently display both the connection with the infinite nuclear matter response as well as the new features introduced by the surface.

Indeed, we believe that our approach yields a realistic description of the role of the surface in the nuclear response: In particular, to our knowledge, the effects associated with the coupling of the spin modes and with the gradient of the density have not been explored before at large momentum transfer.

The paper is organized as follows: Section II reviews those elements of Ref. 17 which are needed for the present study. In Sec. III we give the explicit formulae for the

spin-isospin responses, based on the TW approximation. We also give some insight on the validity of this approximation by investigating the nonlocality in momentum space of $\Pi^0(\mathbf{q},\mathbf{q}';\omega)$.

Section IV contains the results of the present approach utilizing a harmonic oscillator (HO) basis; they are compared with the ones obtained in a semiclassical approximation.[6] In particular, we discuss the validity of the HO basis with respect to a more realistic one. Finally, we compare our results for the transverse response with the existing experimental data.

II. THE SPIN-ISOSPIN NUCLEAR RESPONSE

In Ref. 17 the transverse spin-isospin response is defined as follows:

$$R_T(q,\omega) = -\frac{1}{\pi} \sum_{m,n} \delta_{m,n} \mathrm{Im}\Pi_{m3,n3}(\mathbf{q},\mathbf{q};\omega) , \qquad (2.1)$$

in terms of the spherical "spatial" components $m,n = 0, \pm 1$ of $\Pi_{\mu\nu}(\mathbf{q},\mathbf{q}';\omega)$, whereas the longitudinal one,

$$R_L(q,\omega) = -\frac{1}{2\pi} \mathrm{Im}\Pi_{03,03}(\mathbf{q},\mathbf{q};\omega) , \qquad (2.2)$$

is fixed by the $\mu = \nu = 0$ ("time") components. In (2.1) and (2.2) the index 3 denotes isospin.

By a suitable multipole expansion $\Pi_{\mu\nu}(\mathbf{q},\mathbf{q}';\omega)$ can be factored into a geometrical and a dynamical part (see Ref. 17 for the explicit formulae). The latter obeys, in the RPA framework, the following set of integral equations:

$$[\hat{\Pi}_J^{\mathrm{RPA}}(q,q';\omega)]_{ll'} = [\hat{\Pi}_J^0(q,q';\omega)]_{ll'} + \frac{1}{(2\pi)^3} \int_0^\infty dk\, k^2 \sum_{l_1 l_2} [\hat{\Pi}_J^0(q,k;\omega)]_{ll_1} [U_J(k)]_{l_1 l_2} [\hat{\Pi}_J^{\mathrm{RPA}}(k,q';\omega)]_{l_2 l'} . \qquad (2.3)$$

The first term on the right-hand side (rhs) is the dynamical factor of the independent particle polarization propagator; if the spin-orbit term in the mean field is disregarded, it turns out to be diagonal in the angular momenta, $[\hat{\Pi}_J^0(q,q';\omega)]_{ll'} = \delta_{ll'} \hat{\Pi}_l^0(q,q';\omega)$, and reads (the indices p and h indicate particle and hole, respectively)

$$\hat{\Pi}_l^0(q,q';\omega) = 16\pi \sum_{\substack{n_p l_p \\ n_h l_h}} (2l_p+1)(2l_h+1) \begin{pmatrix} l_p & l_h & l \\ 0 & 0 & 0 \end{pmatrix}^2 \mathscr{I}_{ln_p l_p n_h l_h}(q)$$

$$\times \left[\frac{1}{\hbar\omega - (\epsilon_{n_p l_p} - \epsilon_{n_h l_h}) + i\eta} - \frac{1}{\hbar\omega + (\epsilon_{n_p l_p} - \epsilon_{n_h l_h}) - i\eta} \right] \mathscr{I}_{ln_p l_p n_h l_h}(q') , \qquad (2.4)$$

where

$$\mathscr{I}_{ln_p l_p n_h l_h}(q) = q \int_0^\infty dr\, r^2 j_l(qr) R_{n_p l_p}(r) R_{n_h l_h}(r) . \qquad (2.5)$$

In the above expression the $R_{nl}(r)$ are the radial wave functions, belonging to the eigenvalues ϵ_{nl}. In principle, they should be calculated self-consistently. In practice, we shall use the eigenfunctions of a harmonic oscillator with the strength fixed by the experimental size of the

system. They should at least contain the information on the confinement of the system.

In the following $\hat{\Pi}^0$ will also include the Δ-h propagator, assuming for the isobar the same mean field as for the nucleons.

Now when the nuclear spin-isospin responses (2.1) and (2.2) are explicitly expressed through the $\hat{\Pi}_J^{\mathrm{RPA}}$ components diagonal in momentum space, they turn out to be given by the following combinations:

$$R_T(q,\omega) = -\frac{1}{16\pi^2} \sum_{J=1}^{\infty} ((J+1)\mathrm{Im}[\hat{\Pi}_J^{\mathrm{RPA}}(q,\omega)]_{J-1,J-1} + \sqrt{J(J+1)}\mathrm{Im}\{[\hat{\Pi}_J^{\mathrm{RPA}}(q,\omega)]_{J-1,J+1} + [\hat{\Pi}_J^{\mathrm{RPA}}(q,\omega)]_{J+1,J-1}\}$$

$$+ (2J+1)\mathrm{Im}[\hat{\Pi}_J^{\mathrm{RPA}}(q,\omega)]_{J,J} + J\,\mathrm{Im}[\hat{\Pi}_J^{\mathrm{RPA}}(q,\omega)]_{J+1,J+1}) \tag{2.6}$$

and

$$R_L(q,\omega) = -\frac{1}{8\pi^2} \sum_{J=0}^{\infty} (J\,\mathrm{Im}[\hat{\Pi}_J^{\mathrm{RPA}}(q,\omega)]_{J-1,J-1} - \sqrt{J(J+1)}\mathrm{Im}\{[\hat{\Pi}_J^{\mathrm{RPA}}(q,\omega)]_{J-1,J+1} + [\hat{\Pi}_J^{\mathrm{RPA}}(q,\omega)]_{J+1,J-1}\}$$

$$+ (J+1)\mathrm{Im}[\hat{\Pi}_J^{\mathrm{RPA}}(q,\omega)]_{J+1,J+1}) \ . \tag{2.7}$$

In the noninteracting case, $(\hat{\Pi}_J^0)_{ll'}$ being diagonal, (2.6) and (2.7) reduce to

$$R_T^0(q,\omega) = -\frac{1}{16\pi^2} \sum_{J=1}^{\infty} [(J+1)\mathrm{Im}\hat{\Pi}_{J-1}^0(q,\omega) + J\,\mathrm{Im}\hat{\Pi}_{J+1}^0(q,\omega) + (2J+1)\mathrm{Im}\hat{\Pi}_J^0(q,\omega)] \tag{2.8}$$

and

$$R_L^0(q,\omega) = -\frac{1}{8\pi^2} \sum_{J=0}^{\infty} [J\,\mathrm{Im}\hat{\Pi}_{J-1}^0(q,\omega) + (J+1)\mathrm{Im}\hat{\Pi}_{J+1}^0(q,\omega)] \ . \tag{2.9}$$

It can be shown, with the help of (2.4), that the two expressions (2.8) and (2.9), in fact, coincide.

The problem of calculating the nuclear spin-isospin responses is thus reduced to the one of solving the integral equation (2.3). We will pursue this task in the present paper, with the following parametrization of the spin-isospin particle-hole interaction:[17]

$$[U_J(k)]_{l_1 l_2} = a_{Jl_1} a_{Jl_2} V_L(k) + (\delta_{l_1 l_2} - a_{Jl_1} a_{Jl_2}) V_T(k) \ . \tag{2.10}$$

In (2.10),

$$a_{Jl} = (-1)^l \sqrt{2l+1} \begin{vmatrix} l & 1 & J \\ 0 & 0 & 0 \end{vmatrix} \ , \tag{2.11}$$

$$V_L(k) = \Gamma_\pi^2(k) \frac{f_\pi^2}{\mu_\pi^2} \left[\frac{g'}{k^2} - \frac{1}{k^2 + \mu_\pi^2} \right] \ , \tag{2.12}$$

and

$$V_T(k) = \Gamma_\pi^2(k) \frac{f_\pi^2}{\mu_\pi^2} \frac{g'}{k^2} - \Gamma_\rho^2(k) \frac{f_\rho^2}{\mu_\rho^2} \frac{1}{k^2 + \mu_\rho^2} \ . \tag{2.13}$$

In these formulae g' is the Landau-Migdal parameter, $f_\pi^2/4\pi\hbar c = 0.08$, $f_\rho^2/\mu_\rho^2 = 2.18(f_\pi^2/\mu_\pi^2)$, and $\Gamma_{\pi(\rho)}(k)$ is the usual dipole form factor of the $\pi(\rho)NN$ vertex (we shall use the cutoffs $\Lambda_\pi = 1.3$ GeV and $\Lambda_\rho = 2.0$ GeV, respectively).

III. SOLUTION OF THE RPA EQUATIONS

If translational invariance holds, then $\hat{\Pi}_J^0(q,k;\omega)$ [being proportional to $\delta(q-k)$] picks out only one momentum in the integral of Eq. (2.3), thus reducing the system of coupled equations to algebraic form. It is conceivable that for a large enough nucleus $\hat{\Pi}_J^0(q,k;\omega)$ will retain a fairly diagonal behavior, being peaked around $q = k$. If this is the case, then only a rather narrow band of momenta will effectively contribute to the integrals one encounters when considering the subsequent iterations of Eq. (2.3). This property is exploited in the method of Toki and Weise.[18]

Indeed, according to them, it is possible to reduce the entire problem to algebraic form, providing that the "diagonal" behavior of $\hat{\Pi}_J^0$ is sufficient to invoke the mean value theorem in the first order iteration. More specifically, one has to find an average momentum $\bar{q}$ such that

$$\int_0^\infty \frac{dk\,k^2}{(2\pi)^3} \sum_{l_1 l_2} [\hat{\Pi}_J^0(q,k;\omega)]_{ll_1} [U_J(k)]_{l_1 l_2} [\hat{\Pi}_J^0(k,q';\omega)]_{l_2 l'} = \gamma \frac{\bar{q}^2}{(2\pi)^3} \sum_{l_1 l_2} [\hat{\Pi}_J^0(q,\bar{q};\omega)]_{ll_1} [U_J(\bar{q})]_{l_1 l_2} [\hat{\Pi}_J^0(\bar{q},q';\omega)]_{l_2 l'}$$

$$\simeq \gamma \frac{\bar{q}^2}{(2\pi)^3} \sum_{l_1 l_2} [\hat{\Pi}_J^0(q,q';\omega)]_{ll_1} [U_J(\bar{q})]_{l_1 l_2} [\hat{\Pi}_J^0(\bar{q},\bar{q};\omega)]_{l_2 l'} \ , \tag{3.1}$$

where $\gamma \simeq \pi/R$ (R being the rms radius of the nucleus) roughly corresponds to the range of nonlocality in momentum space.

While the first step in (3.1) directly follows from the mean value theorem, the subsequent one, which is the key point for the evaluation of the higher order iterations, is not trivial and will be reviewed briefly in Appendix A. There it is shown that the approximation (3.1) allows one to replace (2.3) with the matrix equation:

$$[\hat{\Pi}_J^{\mathrm{RPA}}(q,q';\omega)]_{ll'} \simeq [\hat{\Pi}_J^0(q,q';\omega)]_{ll'} + \frac{\gamma \bar{q}^2}{(2\pi)^3} \sum_{l_1 l_2} [\hat{\Pi}_J^{\mathrm{RPA}}(q,q';\omega)]_{ll_1} [U_J(\bar{q})]_{l_1 l_2} [\hat{\Pi}_J^0(\bar{q},\bar{q};\omega)]_{l_2 l'} \ . \tag{3.2}$$

As it stands (3.2) is, however, an oversimplification. Indeed, for fixed J five coupled (through the tensor interaction mediated by the pion and the rho) integral equations stem from (2.3): Thus, *a priori*, one should introduce five average momenta $\bar{q}_J(l,l')$. But then, the reduction of (2.3) to algebraic form is no longer feasible since the higher order iterations of each $[\hat{\Pi}_J^{RPA}(q,q';\omega)]_{ll'}$ would bring into play all the $\bar{q}_J(l,l')$ with increasing complexity.

We have thus decided to disregard the differences, for a given J, among the various $\bar{q}_J(l,l')$. More precisely, we fix the unique $\bar{q}_J$ directly from *the first order approximation for the responses (2.6) and (2.7)*, thus avoiding the further problem connected with the actual existence of two $\bar{q}_J$, arising from the real and imaginary part of (3.1).[19]

In this framework the two responses are given by the following expressions:

$$R_T(q,\omega) = -\frac{1}{16\pi^2}\text{Im}\sum_{J=1}^{\infty}\left\{\frac{(2J+1)\hat{\Pi}_J^0(q,\omega)}{1-\frac{\gamma\bar{q}^2}{(2\pi)^3}V_T(\bar{q})\hat{\Pi}_J^0(\bar{q},\omega)} + \frac{(J+1)\hat{\Pi}_{J-1}^0(q,\omega)}{1-\frac{\gamma\bar{q}^2}{(2\pi)^3}V_T(\bar{q})\hat{\Pi}_{J-1}^0(\bar{q},\omega)+\frac{J}{2J+1}\mathscr{F}_{J+1}(\bar{q},\omega)}\right.$$

$$\left.+\frac{J\hat{\Pi}_{J+1}^0(q,\omega)}{1-\frac{\gamma\bar{q}^2}{(2\pi)^3}V_T(\bar{q})\hat{\Pi}_{J+1}^0(\bar{q},\omega)+\frac{J+1}{2J+1}\mathscr{F}_{J-1}(\bar{q},\omega)}\right\}, \tag{3.3}$$

with

$$\mathscr{F}_{J-1}(p,\omega) = \frac{\gamma p^2}{(2\pi)^3}[V_T(p)-V_L(p)]\frac{\hat{\Pi}_{J+1}^0(p,\omega)-\hat{\Pi}_{J-1}^0(p,\omega)}{1-\frac{\gamma p^2}{(2\pi)^3}V_L(p)\hat{\Pi}_{J-1}^0(p,\omega)}, \tag{3.4}$$

$$\mathscr{F}_{J+1}(p,\omega) = \frac{\gamma p^2}{(2\pi)^3}[V_T(p)-V_L(p)]\frac{\hat{\Pi}_{J-1}^0(p,\omega)-\hat{\Pi}_{J+1}^0(p,\omega)}{1-\frac{\gamma p^2}{(2\pi)^3}V_L(p)\hat{\Pi}_{J+1}^0(p,\omega)}, \tag{3.5}$$

and

$$R_L(q,\omega) = -\frac{1}{8\pi^2}\text{Im}\sum_{J=0}^{\infty}\left\{\frac{(J+1)\hat{\Pi}_{J+1}^0(q,\omega)}{1-\frac{\gamma\bar{q}^2}{(2\pi)^3}V_L(\bar{q})\hat{\Pi}_{J+1}^0(\bar{q},\omega)+\frac{J}{2J+1}\mathscr{G}_{J-1}(\bar{q},\omega)}\right.$$

$$\left.+\frac{J\hat{\Pi}_{J-1}^0(q,\omega)}{1-\frac{\gamma\bar{q}^2}{(2\pi)^3}V_L(\bar{q})\hat{\Pi}_{J-1}^0(\bar{q},\omega)+\frac{J+1}{2J+1}\mathscr{G}_{J+1}(\bar{q},\omega)}\right\}, \tag{3.6}$$

with

$$\mathscr{G}_{J+1}(\bar{q},\omega) = \mathscr{F}_{J+1}(\bar{q},\omega; V_L \leftrightarrow V_T), \tag{3.7}$$

$$\mathscr{G}_{J-1}(\bar{q},\omega) = \mathscr{F}_{J-1}(\bar{q},\omega; V_L \leftrightarrow V_T). \tag{3.8}$$

In expressions (3.3) and (3.6) a "nuclear-matter-like" partial wave expansion is recovered if the quantities $\mathscr{G}_J$ and $\mathscr{F}_J$ are omitted in the denominators. Their effect should therefore vanish in an infinite system. However, even when $\mathscr{G}_J$ and $\mathscr{F}_J$ are ignored, there remains a trace of the confinement of the system in the replacement $q \rightarrow \bar{q}$

in the denominators.

The terms $\mathscr{G}_J$ and $\mathscr{F}_J$ embody the coupling discussed previously between the $(\sigma\times q)$ and $(\sigma\cdot q)$ spin modes, as well as other contributions stemming from the gradient of the nuclear density. They can be sizable in the range of momenta where $q^2(V_T-V_L)$ is large, i.e., roughly for $0.4 \leq q \leq 2.1$ fm^{-1} (see Fig. 1).

The uncoupled responses are those obtained by letting the complete longitudinal $V_L(k)$ [$V_T(k)$] interaction go to zero in (3.3) [(3.6)].

When this is done, the following expressions are obtained:

$$R_T^{\text{no-coupl}}(q,\omega) = -\frac{1}{16\pi^2}\text{Im}\sum_{J=1}^{\infty}(2J+1)\left[\frac{\hat{\Pi}_J^0(q,\omega)}{1-\frac{\gamma\bar{q}^2}{(2\pi)^3}V_T(\bar{q})\hat{\Pi}_J^0(\bar{q},\omega)}\right.$$

$$\left.+\frac{J\hat{\Pi}_{J+1}^0(q,\omega)+(J+1)\hat{\Pi}_{J-1}^0(q,\omega)}{(2J+1)-\frac{\gamma\bar{q}^2}{(2\pi)^3}V_T(\bar{q})[J\hat{\Pi}_{J+1}^0(\bar{q},\omega)+(J+1)\hat{\Pi}_{J-1}^0(\bar{q},\omega)]}\right] \tag{3.9}$$

and

$$R_L^{\text{no-coupl}}(q,\omega) = -\frac{1}{8\pi^2}\text{Im}\sum_{J=0}^{\infty}(2J+1)\frac{(J+1)\hat{\Pi}_{J+1}^0(q,\omega)+J\hat{\Pi}_{J-1}^0(q,\omega)}{(2J+1)-\frac{\gamma\bar{q}^2}{(2\pi)^3}V_L(\bar{q})[(J+1)\hat{\Pi}_{J+1}^0(\bar{q},\omega)+J\hat{\Pi}_{J-1}^0(\bar{q},\omega)]} . \tag{3.10}$$

Before analyzing the results obtained, it is worthwhile to investigate the nonlocality in momentum space of $\Pi^0_{\mu\nu}(q,q';\omega)$. Indeed, as shown in Appendix A, the TW approximation mostly relies on a well-peaked behavior of Π^0 around $q=q'$.

In order to avoid the detailed analysis of the various multipoles, we focus our attention on the imaginary part of the density-density polarization propagator $(\mu=\nu=0$, "time-component").

At the same time we intend to explore how this quantity is affected by the size of the system. Thus, we display, in Fig. 2, $\text{Im}\Pi^0_{0,0}(\mathbf{q},\mathbf{q}';\omega)$ for fixed $q=1.5$ fm^{-1}, $\hat{\mathbf{q}}\cdot\hat{\mathbf{q}}'=1$, and $\hbar\omega\cong55$ MeV as a function of q' for ^{16}O, ^{40}Ca, and ^{80}Zr.

Notably, the curves are bell shaped, showing a minimum for $q\cong q'$ in the case of the largest nucleus, whereas as the mass number decreases the minimum tends to be shifted to larger q'.

As expected, a substantial shrinking of the nonlocality region is seen to occur as one moves from light to heavy
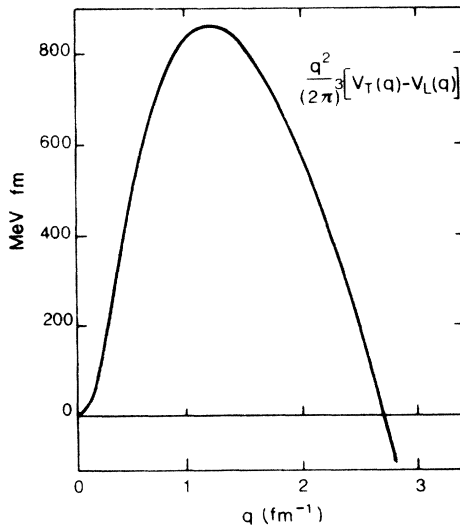
nuclei. This outcome reflects the tendency toward the recovery of translational invariance, although a nonnegligible amount of nonlocality in momentum space (as well as in coordinate space) will always persist due to the existence of the surface, no matter how large the nucleus.

Indeed, the shrinking is more pronounced in going from ^{16}O to ^{40}Ca than from ^{40}Ca to ^{80}Zr. We can characterize the amount of nonlocality by the half-height width $\Delta q'$ of the curves in Fig. 2: It turns out to be 1.2, 1.0, and 0.85 fm^{-1} for ^{16}O, ^{40}Ca, and ^{80}Zr, respectively.

The ratios among these numbers closely follow the corresponding relationship among the surface to volume ratios (S/V) of the considered nuclei: Their relative proportion is 1.36:1:0.79. As a consequence, we can expect that for a nucleus as large as ^{40}Ca the TW approximation is fairly reliable.

Nonlocality in momentum space also depends on the energy ω and tends to decrease as the energy becomes large. Therefore the new effects associated with the gradient of the nuclear density and the consequent mixing between $(\sigma\times\mathbf{q})$ and $(\sigma\cdot\mathbf{q})$ are likely to be more important at low energies, where nonlocality is more appreciable. This will be illustrated in the next section.
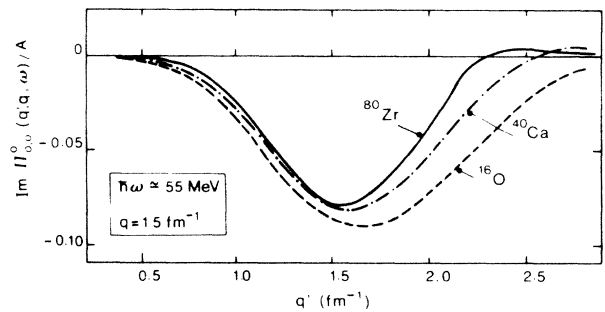

FIG. 1. The difference between the transverse and longitudinal interactions multiplied by $q^2/(2\pi)^3$ as a function of q.

FIG. 2. The imaginary part of $\Pi^0_{0,0}(\mathbf{q},\mathbf{q}';\omega)/A$ at fixed $q=1.5$ fm^{-1}, $\hbar\omega\cong55$ MeV, and $\hat{\mathbf{q}}\cdot\hat{\mathbf{q}}'=1$, as a function of q' for ^{16}O (dashed line), ^{40}Ca (dotted-dashed line), and ^{80}Zr (solid line). The energy is only approximately the same in the three curves since each nucleus keeps its own HO parameter (55 MeV roughly corresponds to $4\hbar\omega_0$ in ^{16}O, $5\hbar\omega_0$ in ^{40}Ca, and $6\hbar\omega_0$ in ^{80}Zr).

IV. RESULTS AND DISCUSSION

We have performed calculations in the case of ^{40}Ca for which experimental data exist. The resulting RPA transverse response is shown in Fig. 3 at $q = 330$ MeV/c, together with the corresponding nuclear matter response. An appreciable difference between the two shows up in the high energy region.

In order to explore the origin of this difference, we have resorted to the semiclassical approach introduced by Schuck,[20] which at least accounts for the confinement of the system. It amounts to the following replacement,

$$R_T = -\frac{2Vq^2}{\pi} \text{Im}\Pi(q,\omega;k_F)$$

$$\Rightarrow -8q^2 \int_0^{R_c} dr\, r^2 \text{Im}\Pi[q,\omega;k_F(r)] , \qquad (4.1)$$

the local Fermi momentum being defined by the equation

$$\frac{\hbar^2 k_F^2(r)}{2m} + W(r) = \frac{\hbar^2(k_F^0)^2}{2m} + W(0) . \qquad (4.2)$$

The value of $k_F^0 \equiv k_F(0)$ is fixed by the condition

$$A = 4\pi \int_0^{R_c} dr\, r^2 \rho(r) . \qquad (4.3)$$

For the potential well $W(r)$ in (4.2), Schuck takes a realistic Woods-Saxon (WS) potential,

$$W_{\text{WS}}(r) = \frac{V_0}{1+\exp[(r-R_0)/a]} , \qquad (4.4)$$

with $V_0 = -50$ MeV, $R_0 = 1.2A^{1/3}$ fm, and $a = 0.5$ fm. In order to facilitate comparison with our results, we shall also consider a harmonic oscillator well (HO),

$$W_{\text{HO}}(r) = V_1 + \tfrac{1}{2}m\omega_0^2 r^2 , \qquad (4.5)$$

with $V_1 = -55$ MeV and $\hbar\omega_0 = 41A^{-1/3}$ MeV. This comparison will allow a test of the shortcomings stemming from the use of the harmonic oscillator model.

The upper limit of integration in (4.1) corresponds to the classical turning point for the single particle motion inside the nucleus and is set by the equation

$$k_F(R_c) = 0 , \qquad (4.6)$$

which, e.g., for the Woods-Saxon well, yields

$$R_c = R_0 + a \ln\left|\frac{V_0}{V_0 + \hbar^2(k_F^0)^2/2m} - 1\right| = 4.85 \text{ fm} . \qquad (4.7)$$

In Fig. 4 we display the semiclassical transverse response (4.1) for a WS and a HO well, compared with the nuclear matter RPA response. Discrepancies with the latter at high energies are present as well in the semiclassical approach. The differences between HO and WS semi-
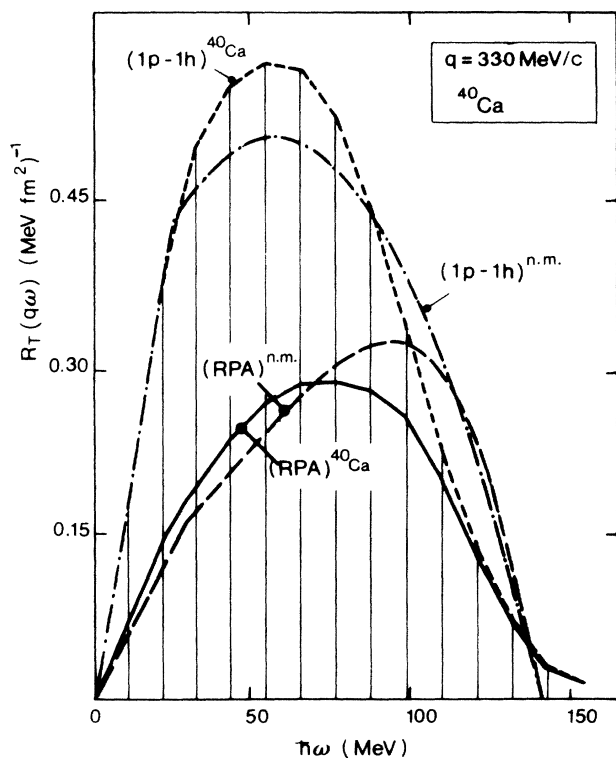

FIG. 3. Free and RPA transverse responses for ^{40}Ca at $q = 330$ MeV/c as a function of $\hbar\omega$. The solid and dotted lines correspond to the finite nucleus calculation; the dotted-dashed and dashed lines correspond to the infinite nuclear matter responses with a Fermi momentum $k_F = 1.2$ fm^{-1}.
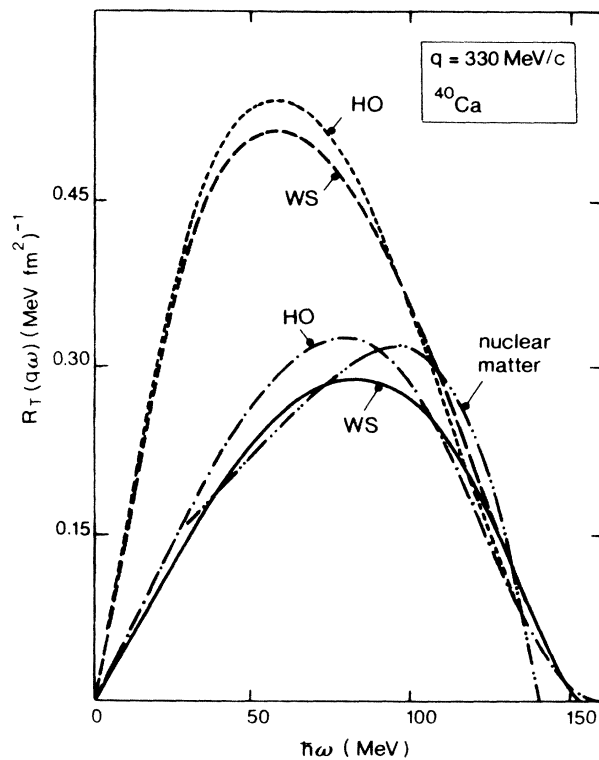

FIG. 4. Free and RPA semiclassical transverse responses for ^{40}Ca at $q = 330$ MeV/c as a function of $\hbar\omega$. The dotted and dashed-dotted lines refer to the HO potential; the dashed and solid lines refer to the WS one. The infinite nuclear matter RPA response (double-dotted dashed line) is the same as in Fig. 3.

classical results provide a feeling of the errors involved in the use of a HO basis with respect to a more realistic one. However, this is the only basis which makes the present RPA calculation feasible.

We remark that the RPA renormalization is weaker for the HO semiclassical response than for the WS one; indeed, the classical turning point for the HO well ($R_c = 5.1$ fm) is larger than the WS one. The corresponding density is then smaller in the region between 2 and 4 fm, where the quantity $r^2\rho(r)$ peaks. Thus, less collectivity is present in the RPA HO response. This feature, however, is not shared by our finite nucleus calculation, which is compared in Fig. 5 with the semiclassical approximation in the HO basis. Both our full RPA, expression (3.3), and the one where the gradient-density terms are omitted, are shown in the figure. The three curves are rather close at low energies, but our results display a more pronounced collectivity in the region of the maximum.

The difference between our two finite nucleus transverse responses is small (at most 10%), showing the moderate influence, in the volume response, of the contribution stemming from the gradient density terms.

Notice that the coupling between $(\boldsymbol{\sigma} \cdot \mathbf{q})$ and $(\boldsymbol{\sigma} \times \mathbf{q})$ has practically no effect here, since at this particular momentum transfer the longitudinal force is relatively small (see also Table I). It should be remarked, however, that this is not a general feature valid for all q. Indeed, for example, at $q = 1.75$ fm^{-1} the influence of the $(\boldsymbol{\sigma} \cdot \mathbf{q})$ coupling in the transverse response may result in an increase of up to 9—10 %. Obviously, the q dependence of this effect has to be traced back to the one of V_L, which is rather pronounced owing to the small pionic mass.

On the contrary, as V_T is generally large, the transverse-longitudinal coupling sizably affects the longitudinal response; this is displayed in Fig. 6, where, together with the full finite nucleus calculation, the noninteracting response and the one without $(\boldsymbol{\sigma} \times \mathbf{q})$ mixing are shown (see also Table II).

These results somehow disagree with previous investigations[21] of the role of the pion (the rho meson) in the transverse (longitudinal) channel.
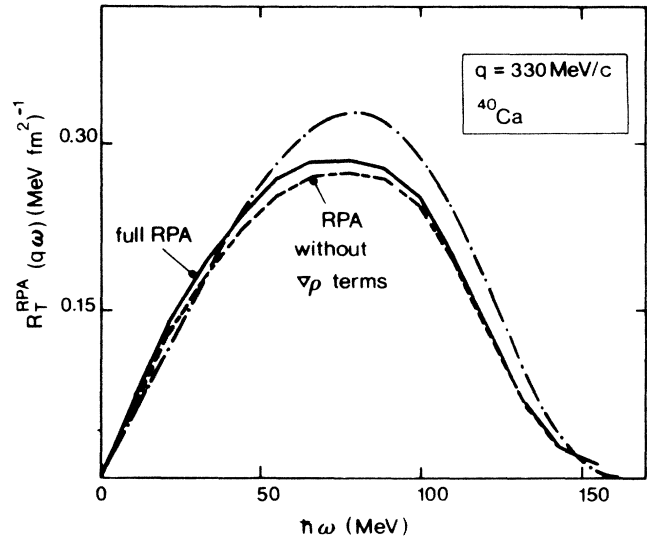
Altogether, the mixing between longitudinal and trans-

FIG. 5. RPA transverse responses for ^{40}Ca at $q = 330$ MeV/c as a function of $\hbar\omega$. The dotted-dashed line is the semiclassical response with the HO potential; the solid line is the full RPA finite nucleus calculation, and the dashed line the one where the gradient density terms are omitted.

verse spin couplings, which occurs through the gradient density terms and which is the new feature of our approach, is thus rather small in the global responses. However, it plays a significant role in the individual multipoles of the responses.

Figures 7(a) and 7(b) show the renormalization factors $(R/R^0)_J$ of the transverse and longitudinal multipoles as a function of J. As expected, the low multipoles which probe the nuclear interior are very collective and display a strong contrast between the longitudinal and transverse channels. On the other hand, collectivity is less pronounced for the higher multipolarities, which are peripheral and thus show less contrast even in the absence of the mixing.

TABLE I. Detailed transverse responses for ^{40}Ca at $q=330$ MeV/c. Column 3 contains the independent particle response, column 4 the full RPA calculation, column 5 $[R_T^{RPA}(1)]$ the one without mixing of $V_L(q)$, and column 6 $[R_T^{RPA}(2)]$ the transverse response without mixing of the gradient density terms. The responses are in $(MeV\,fm^2)^{-1}$. P_1 and P_2 are defined as follows: $P_1 = [R_T^{RPA} - R_T^{RPA}(1)]/R_T^{RPA}$ and $P_2 = [R_T^{RPA} - R_T^{RPA}(2)]/R_T^{RPA}$.

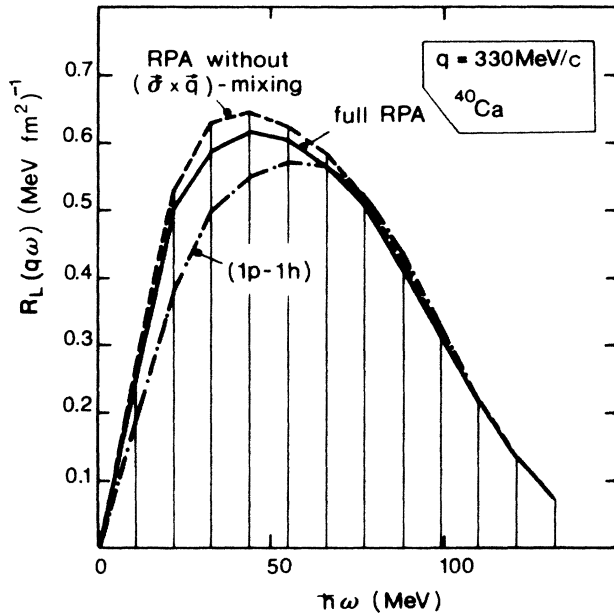| $\hbar\omega$ (MeV)	$\hbar\omega/\hbar\omega_0$	R_T^0	R_T^{RPA}	$R_T^{RPA}(1)$	$R_T^{RPA}(2)$	P_1 (%)	P_2 (%)
11.02	1	0.194	0.072	0.070	0.065	2.62	9.66
22.04	2	0.377	0.141	0.138	0.131	2.06	7.28
33.06	3	0.499	0.192	0.188	0.179	1.89	6.87
44.08	4	0.550	0.234	0.229	0.220	1.85	6.02
55.10	5	0.572	0.265	0.261	0.251	1.62	5.48
66.12	6	0.566	0.282	0.279	0.269	1.24	4.66
77.14	7	0.524	0.284	0.279	0.272	1.00	4.33
88.16	8	0.442	0.277	0.275	0.267	0.61	3.61
99.18	9	0.335	0.251	0.250	0.244	0.32	2.63

FIG. 6. The longitudinal responses of ^{40}Ca at $q=330$ MeV/c as a function of $\hbar\omega$. The dotted-dashed line is the independent particle response, the solid line the full RPA finite nucleus calculation, and the dashed line the one where the mixing of $V_T(q)$ is omitted.
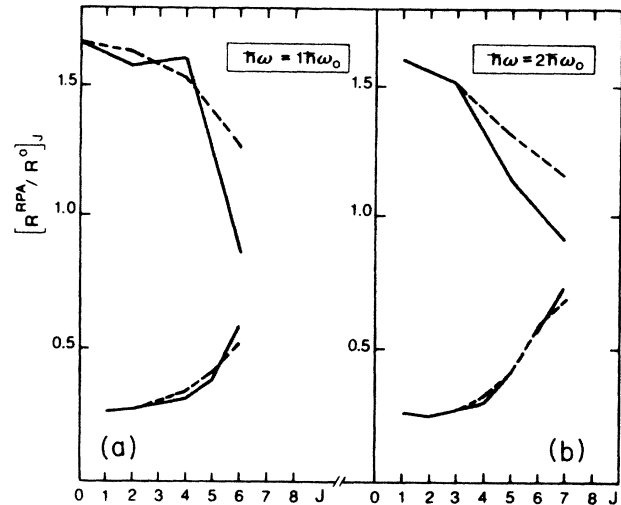
FIG. 7. (a) Ratios of RPA and independent particle multipoles contributing to the finite nucleus responses, at fixed $q=330$ MeV/c and $\hbar\omega=1\hbar\omega_0$ as a function of J. The dashed lines refer to the calculation without $(\sigma\cdot q)$ $[(\sigma\times q)]$ mixing in the transverse (longitudinal) channel. The solid lines refer to the full RPA calculation. Upper and lower curves represent the longitudinal and transverse channels, respectively. (b) The same as (a), but at $\hbar\omega=2\hbar\omega_0$.

The remarkable feature displayed in Figs. 7(a) and 7(b) is that, in contrast to what happens for the low multipoles (and in general for the volume responses), the coupling between $(\sigma\cdot q)$ and $(\sigma\times q)$ is extremely effective for the higher multipoles and produces a suppression of the contrast beyond what would be expected simply from the lowering of the density.

This suggests that the contrast is suppressed for peripheral probes such as (p,p') due to the coupling between the two channels at the nuclear surface. This may give a clue for the interpretation of the Los Alamos experiment,[22] which has revealed no contrast. A detailed evaluation of the surface response requires a specific treatment and will be discussed in a forthcoming paper.[9]

For purposes of illustration, we display in Fig. 8 the ratio between the volume responses, R_L/R_T, with and

without the inclusion of the above discussed mixing, and compare it with the same quantity calculated in nuclear matter.

A sizable reduction of this ratio in the finite system is apparent. There remains, however, some contrast between the two responses, even when the transverse-longitudinal mixing is included. Therefore the present treatment, being limited to the volume responses, is not yet appropriate to account for the Los Alamos experiment, which mainly probes the nuclear surface.

A better testing ground for the present theory is the comparison with the transverse dynamic structure factor, as measured in (e,e') experiments. This quantity is linked to the polarization propagator and to our transverse response function (2.1) by the following definitions (m,n spherical indices):

TABLE II. The same as Table I for the longitudinal responses.

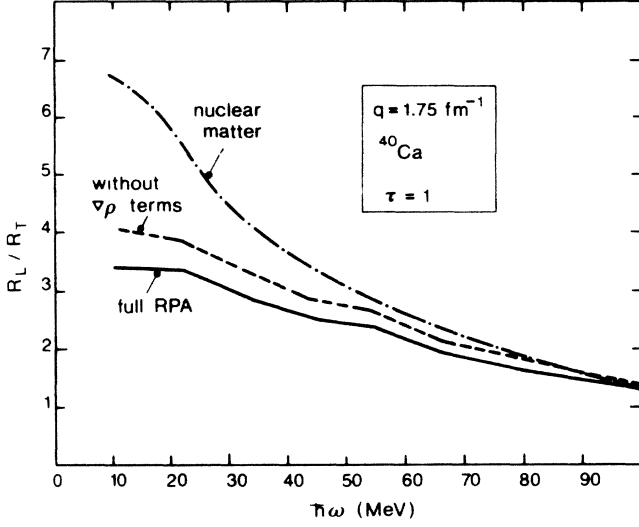| $\hbar\omega$ (MeV)	$\hbar\omega/\hbar\omega_0$	R_L^0	R_L^{RPA}	$R_L^{RPA}(1)$	$R_L^{RPA}(2)$	P_1 (%)	P_2 (%)
11.02	1	0.194	0.266	0.286	0.287	7.72	8.17
22.04	2	0.377	0.502	0.533	0.550	6.16	9.53
33.06	3	0.499	0.592	0.628	0.628	6.18	6.10
44.08	4	0.550	0.618	0.647	0.643	4.71	4.14
55.10	5	0.572	0.607	0.628	0.624	3.46	2.83
66.12	6	0.566	0.566	0.583	0.574	3.15	1.50
77.14	7	0.524	0.512	0.520	0.515	1.66	0.70
88.16	8	0.442	0.417	0.424	0.416	1.53	−0.24
99.18	9	0.335	0.323	0.324	0.322	0.31	−0.28

FIG. 8. The ratio between the RPA longitudinal and transverse responses for ^{40}Ca at $q=1.75$ fm^{-1} as a function of $\hbar\omega_0$. The solid line refers to the full RPA calculation; the dashed line to the one where the gradient density terms are omitted. The dotted-dashed line is the ratio between the infinite nuclear matter responses with $k_F=1.2$ fm^{-1}.
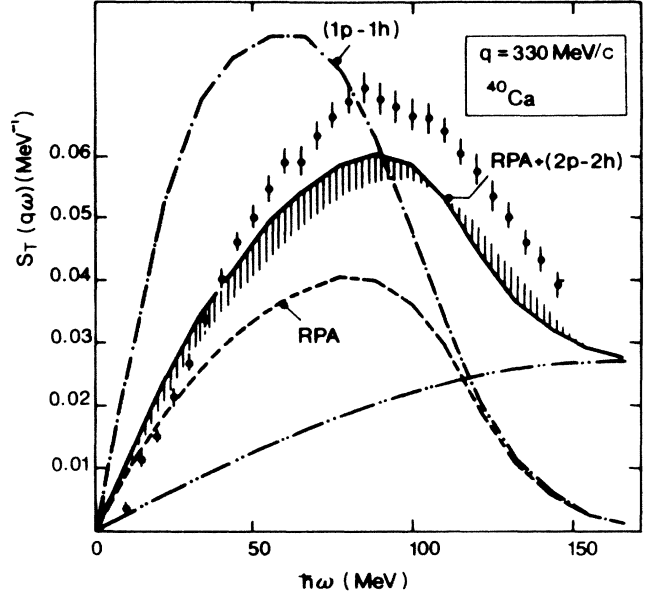

FIG. 9. The transverse dynamic structure factor of ^{40}Ca measured in (e,e') inelastic scattering as a function of $\hbar\omega$, at fixed momentum transfer $q=330$ MeV/c. The experimental points are taken from Ref. 1. The dotted-dashed line refers to the independent particle response, the dashed line to the present RPA calculation, and the solid line is obtained by adding to the latter the 2p-2h contribution (double-dotted-dashed line) of Ref. 3.

$$S_T(\mathbf{q},\omega) = -\frac{\mu_0^2}{e^2}(\mu_p-\mu_n)^2 G_M^2(q_\lambda^2)$$

$$\times \frac{1}{\pi}\sum_{m,n}\left[\delta_{m,n}-(-1)^{m+n}\frac{1}{q^2}q_{-m}q_n\right]$$

$$\times \mathrm{Im}\Pi_{m3,n3}(\mathbf{q},\mathbf{q};\omega)$$

$$= \frac{\mu_0^2}{e^2}(\mu_p-\mu_n)^2 G_M^2(q_\lambda^2)R_T(\mathbf{q},\omega) , \qquad (4.8)$$

μ_0 being the nuclear Bohr magneton, $\mu_p=2.79$, $\mu_n=-1.91$, and

$$G_M(q_\lambda^2) = \frac{1}{[1+(\mathbf{q}^2-\omega^2/c^2)/(18.1 \text{ fm}^{-2})]^2} , \qquad (4.9)$$

the usual electromagnetic γNN form factor. In (4.8) we have neglected the small isoscalar contribution.

We have calculated (4.8) for ^{40}Ca at $q=330$, 370, and 410 MeV/c. Our results are reported in Figs. 9, 10, and 11, respectively, where they are compared with the inclusive experiments of Saclay.[3] The dashed area in Fig. 9 represents the "theoretical error" associated with the use of a HO basis rather then a WS one, deduced in the semiclassical approach as was illustrated in Fig. 3.

First, we note that the independent particle response does not reproduce the experimental data, as already remarked in Ref. 17. The RPA response, instead, when added to the 2p-2h contribution of Ref. 5, gives satisfactory agreement with the data.

The best agreement is obtained at 410 MeV/c, whereas at 330 MeV/c strength is clearly missing near the max-

imum of the response, whose position is, however, correctly reproduced. This outcome could reflect a q dependence of the Landau-Migdal parameter g' (here we use the constant value $g'=0.7$), which should decrease at low momenta. The agreement at 410 MeV/c is suggestive of the persistence of a mild collective behavior even at this momentum transfer.

The theoretical curves of Figs. 9–11 show some extra strength, with respect to the experiment, on the low energy side. This failure does not appear in the semiclassical response, which utilizes a WS potential. This can be seen in Fig. 12, where the semiclassical transverse structure
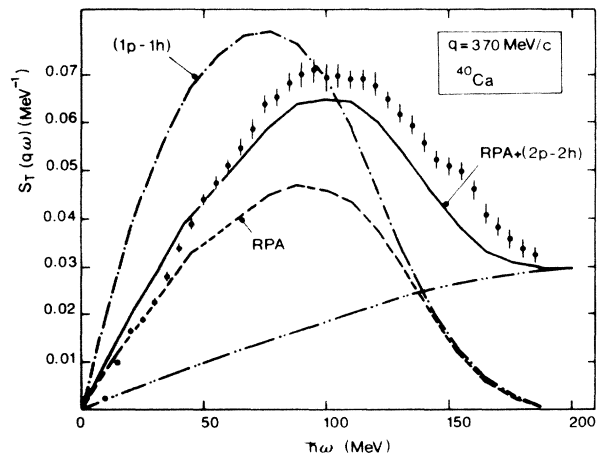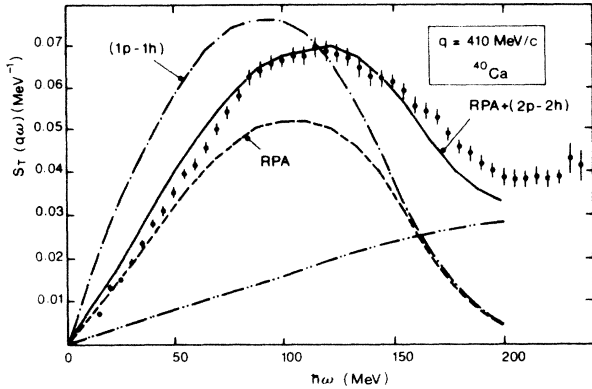

FIG. 10. The same as Fig. 9, at $q=370$ MeV/c.

FIG. 11. The same as Fig. 9, at $q=410$ MeV/c.

factor

$$S_T^{sc}(q,\omega) = -2\frac{\hbar^2 q^2}{m^2 c^2}(\mu_p - \mu_n)^2 G_M^2(q_\lambda^2)$$

$$\times \int_0^{R_c} dr\, r^2 \mathrm{Im}\Pi[q,\omega;k_F(r)] \qquad (4.10)$$

is displayed together with the full finite nucleus calculation. However, (4.10) neglects the coupling between the spin modes as well as the gradient of the nuclear density, which increase—by a modest but (at low energy) significant amount—the finite nucleus response.

The most likely explanation for the origin of this discrepancy is that our treatment of the 2p-2h excitations overestimates their importance at low energies, as it
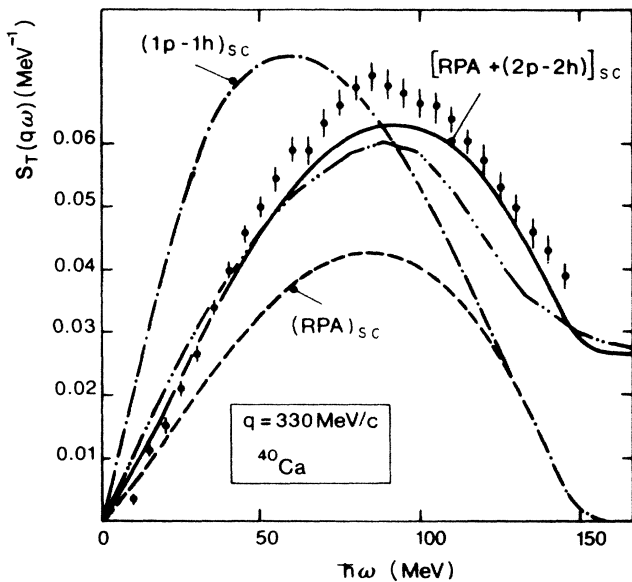

FIG. 12. The transverse dynamic structure factor of ^{40}Ca measured in (e,e') inelastic scattering as a function of $\hbar\omega$, at fixed momentum transfer $q=330$ MeV/c. The experimental points are taken from Ref. 1. The theoretical curves are obtained in the semiclassical approach with a WS potential. The dotted-dashed line is the free response, the dashed line the RPA one, and the solid line is the sum of the latter with the 2p-2h contribution of Ref. 3. For comparison, the finite nucleus total response of Fig. 9 is also displayed (double-dotted-dashed line).

neglects RPA correlations in this sector.

In concluding this section we note that with the present theory a reasonable fit to the experimental data has been obtained. The remaining discrepancies could be eliminated by the momentum dependence of g' and by a proper account for RPA correlations in the 2p-2h response.

Nevertheless, one should not forget that we do not solve *exactly*, but only *approximately*, the RPA equations: Although we believe that our results are good, we cannot claim that they are not subject to some uncertainty. Indeed, beyond the algebraic reduction of the exact integral equations, we have neglected here, as in the nuclear matter framework, the exchange matrix elements of the p-h force (although these are partially included in g'). However, it may be worth pointing out that even the present approach, which implies (in order to set the value of the corresponding $\bar{q}_J$) the evaluation of the exact $\Pi_J^1(q,q;\omega)$ for each ω, q, and J would not have been practical without the use of a Cray computer.

V. CONCLUSIONS

In this paper we have presented a RPA evaluation of the spin-isospin response function for a finite system. For this purpose we have utilized the approximation scheme suggested by Toki and Weise which leads to analytical expressions for the responses themselves. This approach is particularly interesting since it allows a direct investigation of the new features introduced by the finite size of the system: namely the mixing between the $(\sigma \cdot q)$ and $(\sigma \times q)$ couplings and the influence of the nonuniform density, which manifest themselves in terms involving the density gradient. These features have not been included in previous treatments.

We have given some arguments about the reliability of the TW approximation by analyzing the nonlocality in momentum space of $\Pi^0(q,q';\omega)$, which turns out to be sufficiently peaked to justify the approximation. For the same purpose we have compared the present theory with a semiclassical one, which embodies some of the effects associated with a nonuniform density, and we have found the corresponding volume responses to be rather close to each other. They both show some differences relative to the nuclear matter response, particularly at high energy.

The semiclassical treatment also gave us a feeling for the dependence of the theory on the single-particle basis by comparing the semiclassical responses obtained with the HO and WS potentials. Indeed, some failures of our finite nucleus calculation in the description of the experimental data would tend to be cured by the use of a more realistic WS basis.

Altogether, the comparison of the present RPA theory (added to the 2p-2h contribution) with the transverse structure function measured in (e,e') experiments is satisfactory. Some of the discrepancies suggest a mild momentum dependence of g' (which should be lowered at small q).

We have paid particular attention to the mixing between the $(\sigma \cdot q)$ and $(\sigma \times q)$ couplings and to the gradient density terms, which are both ignored in our nuclear matter and semiclassical treatments. Both of them tend to lower the collectivity of the RPA responses. In the

overall volume responses their effect remains small, of the order of 10% at most. The influence of the longitudinal coupling in the transverse response is q dependent, reflecting the strong momentum dependence of the longitudinal p-h interaction.

The detailed analysis of the mixing between the two spin couplings on the separate multipoles of the response reveals interesting features: its influence is small for the low multipoles, which probe the nuclear interior. Conversely, the longitudinal-transverse mixing produces large modifications in the high multipoles, which are peripheral. Its effect tends to equalize the RPA renormalization of the longitudinal and transverse multipoles, thus suppressing the contrast between them. Since these peripheral multipoles are the relevant ones in the surface responses [as the ones probed in (p,p') scattering], one cannot rule out *a priori* a severe reduction of the contrast between the longitudinal and transverse surface responses while at the same time finding strong collective effects in the volume spin-isospin responses.

We wish to thank Dr. R. Mason for his valuable help in computational problems.

APPENDIX A

We briefly review here the hypothesis underlying the approximation method suggested by Toki and Weise.[18]

Let us then consider the first order integral, Eq. (3.1),

$$\hat{\Pi}_J^{(1)}(q,q';\omega) = \frac{1}{(2\pi)^3} \int_0^\infty dk\, k^2 \hat{\Pi}_J^0(q,k;\omega)$$
$$\times U_J(k)\hat{\Pi}_J^0(k,q';\omega)\ , \quad \text{(A1)}$$

and assume that the nonlocal behavior in momentum space of $\hat{\Pi}_J^0(q,q';\omega)$ can be reproduced as follows:

$$\hat{\Pi}_J^0(q,q';\omega) = g(q,\omega)d_J(q-q')g(q',\omega)\ . \quad \text{(A2)}$$

In the above, $g(q,\omega)$ is an appropriate function which we do not need to specify, whereas $d_J(q-q')$ is a distribution function centered at the origin; it satisfies the following conditions:

$$d_J(0) = 1\ , \quad \text{(A3)}$$

$$\int_0^\infty dk\, d_J(q-k)d_J(k-q') = d_J(q-q')\ . \quad \text{(A4)}$$

Formula (A2) implies that $\hat{\Pi}_J^0(q,q';\omega)$ has a well defined minimum at $q = q'$, being fairly symmetrical around it. If this is the case, then (A1) becomes

$$\hat{\Pi}_J^{(1)}(q,q';\omega) = \frac{1}{(2\pi)^3}g(q,\omega)g(q',\omega)\int_0^\infty dk\, k^2 g(k,\omega)U_J(k)g(k,\omega)d_J(q-k)d_J(k-q')$$
$$\simeq \frac{\gamma}{(2\pi)^3}\bar{q}^2 g(\bar{q},\omega)g(\bar{q},\omega)U_J(\bar{q})g(q,\omega)g(q',\omega)\int_0^\infty dk\, d_J(q-k)d_J(k-q')\ , \quad \text{(A5)}$$

where the mean value theorem has been utilized. Using (A3) and (A4), we can immediately obtain

$$\hat{\Pi}_J^{(1)}(q,q';\omega) \cong \frac{\gamma\bar{q}^2}{(2\pi)^3}\hat{\Pi}_J^0(\bar{q},\bar{q};\omega)U_J(\bar{q})\hat{\Pi}_J^0(q,q';\omega)\ , \quad \text{(A6)}$$

which coincides with the last expression in (3.1).

The same steps can now be performed in the subsequent iterations of the integral equation (2.3); for purposes of illustration, we shall consider the second order one:

$$\hat{\Pi}_J^{(2)}(q,q';\omega) = \frac{1}{(2\pi)^3}\int_0^\infty dk\, k^2 \hat{\Pi}_J^0(q,k;\omega)U_J(k)\hat{\Pi}_J^{(1)}(k,q';\omega)\ . \quad \text{(A7)}$$

With the help of (A6) one immediately obtains

$$\hat{\Pi}_J^{(2)}(q,q';\omega) \simeq \frac{\gamma\bar{q}^2}{(2\pi)^3}\hat{\Pi}_J^0(\bar{q},\bar{q};\omega)U_J(\bar{q})\int_0^\infty \frac{dk\, k^2}{(2\pi)^3}\hat{\Pi}_J^0(q,k;\omega)U_J(k)\hat{\Pi}_J^0(k,q';\omega)$$
$$\simeq \left[\frac{\gamma\bar{q}^2}{(2\pi)^3}\hat{\Pi}_J^0(\bar{q},\bar{q};\omega)U_J(\bar{q})\right]^2 \hat{\Pi}_J^0(q,q';\omega)\ , \quad \text{(A8)}$$

and thus the approximate algebraic form (3.2) for the RPA equations is recovered.

There remains a subtle point in going from (A7) to (A8): Indeed, the $\bar{q}$ value introduced, in (A5), by the mean value theorem, depends, in principle, upon q and q'. On the rhs of (A7) one should use, therefore, a $\bar{q}(k,q')$ which, in turn, would inhibit the subsequent step. However, the integrand of Eq. (A5) depends upon q and q' through the product $d_J(q-k)d_J(k-q')$, which, owing to the well peaked behavior of the distribution function, will favor values of k within a relatively narrow band around $q \approx q'$. As a consequence, $\bar{q}$ will be close to q (or q') and the first equality in (A8) appears to be justified.

APPENDIX B

We derive here, using an harmonic oscillator basis and the interaction (2.10), the exact analytic expression for the first order polarization propagator $(\hat{\Pi}^1)_{ll'}$. In particular, we consider its imaginary part, which is the one actually used for the determination of $\bar{q}_J$. It reads

$$\text{Im}[\hat{\Pi}_J^{(1)}(q,q';\omega)]_{ll'} \equiv \frac{1}{(2\pi)^3} \int_0^\infty dk\, k^2 [U_J(k)]_{ll'}[\text{Im}\hat{\Pi}_l^0(q,k;\omega)\text{Re}\hat{\Pi}_{l'}^0(k,q';\omega) + \text{Re}\hat{\Pi}_l^0(q,k;\omega)\text{Im}\hat{\Pi}_{l'}^0(k,q';\omega)] , \tag{B1}$$

which, by defining

$$\Delta_{\text{ph}} = -\pi\delta[\hbar\omega - (\epsilon_{n_p l_p} - \epsilon_{n_h l_h})] = -\frac{\pi}{\hbar\omega_0}\delta(\Delta N - N_p + N_h) \tag{B2}$$

and

$$E_{\text{ph}} = \begin{cases} -\dfrac{1}{2\hbar\omega} & \text{if } \hbar\omega = \epsilon_{n_p l_p} - \epsilon_{n_h l_h} , \\[2mm] \dfrac{2(\epsilon_{n_p l_p} - \epsilon_{n_h l_h})}{(\hbar\omega)^2 - (\epsilon_{n_p l_p} - \epsilon_{n_h l_h})^2} & \text{if } \hbar\omega \neq \epsilon_{n_p l_p} - \epsilon_{n_h l_h} , \end{cases} \tag{B3}$$

where $N_{p,h} = 2n_{p,h} + l_{p,h} + \frac{3}{2}$ and $\hbar\omega_0$ is the harmonic oscillator parameter, can be recast in the following form:

$$\text{Im}[\hat{\Pi}_J^{(1)}(q,q';\omega)]_{ll'} = \frac{32}{\pi} \sum_{\substack{n_p l_p \\ n_h l_h}} \sum_{\substack{n_p' l_p' \\ n_h' l_h'}} (2l_p+1)(2l_h+1)(2l_p'+1)(2l_h'+1) \begin{bmatrix} l_p & l_h & l \\ 0 & 0 & 0 \end{bmatrix}^2 \begin{bmatrix} l_p' & l_h' & l' \\ 0 & 0 & 0 \end{bmatrix}^2$$

$$\times \mathscr{F}_{ln_p l_p n_h l_h}(q)\mathscr{F}_{l'n_p' l_p' n_h' l_h'}(q')(\Delta_{\text{ph}}E_{\text{p'h'}} + E_{\text{ph}}\Delta_{\text{p'h'}})$$

$$\times \int_0^\infty dk\, k^2 [U_J(k)]_{ll'}\mathscr{F}_{ln_p l_p n_h l_h}(k)\mathscr{F}_{l'n_p' l_p' n_h' l_h'}(k) . \tag{B4}$$

The above integral, recalling the analytic expression for $\mathscr{F}_{ln_p l_p n_h l_h}(k)$ given in the Appendix of Ref. 17 and neglecting the k dependence of the $\pi(\rho)NN$ vertex form factor, turns out to be of the type

$$I(2n) = \int_0^\infty dk\, e^{-k^2/2\nu}\frac{1}{k^2+b^2}k^{2n} , \tag{B5}$$

b ($=\mu_\pi$ or μ_ρ) being a constant, n an integer ≥ 1, and $\nu = m\omega_0/\hbar$ and can be analytically evaluated by utilizing the following, easily established, recursion relation,

$$I(2n) = \left[\frac{\pi\nu}{2}\right]^{1/2}\nu^{n-1}(2n-3)!! - b^2 I(2n-2) , \tag{B6}$$

together with the well-known formula[23]

$$I(0) = \frac{\pi}{2b}e^{b^2/2\nu}\text{erfc}\left[\frac{b}{\sqrt{2\nu}}\right] . \tag{B7}$$

The definition

$$\text{erfc}(x) = \frac{2}{\sqrt{\pi}}\int_x^\infty e^{-t^2}dt \tag{B8}$$

has been used for the error function.
The final result reads

$$\text{Im}[\hat{\Pi}_J^{(1)}(q,q';\omega)]_{ll'}$$

$$= \frac{32\nu}{2^{(l+l')/2}\pi}\left[\frac{\pi\nu}{2}\right]^{1/2}\sum_{\substack{n_p l_p \\ n_h l_h}} \sum_{\substack{n_p' l_p' \\ n_h' l_h'}} (2l_p+1)(2l_h+1)(2l_p'+1)(2l_h'+1)$$

$$\times \begin{bmatrix} l_p & l_h & l \\ 0 & 0 & 0 \end{bmatrix}^2 \begin{bmatrix} l_p' & l_h' & l' \\ 0 & 0 & 0 \end{bmatrix}^2 \mathscr{F}_{ln_p l_p n_h l_h}(q)\mathscr{F}_{l'n_p' l_p' n_h' l_h'}(q')$$

$$\times (\Delta_{ph} E_{p'h'} + E_{ph} \Delta_{p'h'}) \left[\frac{sf(l_p,n_p) sf(l_h,n_h)}{2^{n_p+n_h} n_p! n_h!} \frac{sf(l'_p,n'_p) sf(l'_h,n'_h)}{2^{n'_p+n'_h} n'_p! n'_h!} \right]^{1/2}$$

$$\times \sum_{k=0}^{n_p} \sum_{k'=0}^{n_h} \sum_{n=0}^{n'_p} \sum_{n'=0}^{n'_h} \begin{bmatrix} n_p \\ k \end{bmatrix} \begin{bmatrix} n_h \\ k' \end{bmatrix} \begin{bmatrix} n'_p \\ n \end{bmatrix} \begin{bmatrix} n'_h \\ n' \end{bmatrix}$$

$$\times \frac{(-1)^{k+k'+n+n'} sf(l,M) sf(l',M')}{sf(l_p,k) sf(l_h,k') sf(l'_p,n) sf(l'_h,n')}$$

$$\times \sum_{m=0}^{M} \sum_{m'=0}^{M'} (-\tfrac{1}{2})^{m+m'} \begin{bmatrix} M \\ m \end{bmatrix} \begin{bmatrix} M' \\ m' \end{bmatrix} \frac{1}{sf(l,m) sf(l',m')} [V_J(N)]_{ll'} ,$$

$$\text{(B9)}$$

where

$$[V_J(N)]_{ll'} = a_\pi g' \delta_{ll'} (2N-1)!! + a_\rho (a_{Jl} a_{Jl'} - \delta_{ll'})$$

$$\times \left[\sum_{s=0}^{N} (-1)^s \left[\frac{\mu_\rho^2}{\nu} \right]^s (2N-2s-1)!! + \left[-\frac{\mu_\rho^2}{\nu} \right]^{N+1} \left[\frac{\pi\nu}{2\mu_\rho^2} \right]^{1/2} e^{\mu_\rho^2/2\nu} \mathrm{erfc} \left[\frac{\mu_\rho}{\sqrt{2\nu}} \right] \right]$$

$$- a_\pi a_{Jl} a_{Jl'} \left[\sum_{s=0}^{N} (-1)^s \left[\frac{\mu_\pi^2}{\nu} \right]^s (2N-2s-1)!! + \left[-\frac{\mu_\pi^2}{\nu} \right]^{N+1} \left[\frac{\pi\nu}{2\mu_\pi^2} \right]^{1/2} e^{\mu_\pi^2/2\nu} \mathrm{erfc} \left[\frac{\mu_\pi}{\sqrt{2\nu}} \right] \right] ,$$

$$\text{(B10)}$$

and the definitions

$$sf(l,n) = (2l+2n+1)!! , \quad \text{(B11)}$$

$$N = m + m' + 1 + (l+l')/2 , \quad \text{(B12a)}$$

$$M = (l_p + l_h - l)/2 + k + k' , \quad \text{(B12b)}$$

$$M' = (l'_p + l'_h - l')/2 + n + n' , \quad \text{(B12c)}$$

$$a_\pi = \Gamma_\pi^2(q^2) \frac{f_\pi^2}{\mu_\pi^2} , \quad \text{(B12d)}$$

$$a_\rho = \Gamma_\rho^2(q^2) \frac{f_\rho^2}{\mu_\rho^2} \quad \text{(B12e)}$$

have been used.

[1]J. Meyer-ter-Vehn, Phys. Rep. **74**, 323 (1981).

[2]E. Oset, H. Toki, and W. Weise, Phys. Rep. **83**, 281 (1982).

[3]Z. E. Meziani et al., Phys. Rev. Lett. **54**, 1233 (1985).

[4]W. M. Alberico, M. Ericson, and A. Molinari, Nucl. Phys. **A379**, 429 (1982).

[5]W. M. Alberico, M. Ericson, and A. Molinari, Ann. Phys. (N.Y.) **154**, 356 (1984).

[6]U. Stroth, R. W. Hasse, P. Schuck, W. M. Alberico, A. Molinari, and M. Ericson, Phys. Lett. **156B**, 291 (1985).

[7]J. Delorme, M. Ericson, A. Figureau, and C. Thevenet, Ann. Phys. (N.Y.) **102**, 273 (1976).

[8]H. Esbensen and G. F. Bertsch, Ann. Phys. (N.Y.) **157**, 255 (1984).

[9]W. M. Alberico, A. De Pace, M. Ericson, M. B. Johnson, and A. Molinari, submitted to Phys. Lett. B.

[10]J. Speth, V. Klemt, J. Wambach, and G. E. Brown, Nucl.

Phys. **A343**, 382 (1980).

[11]G. E. Brown and M. Rho, Nucl. Phys. **A372**, 397 (1981).

[12]S. O. Bäckman, G. E. Brown, V. Klemt, and J. Speth, Nucl. Phys. **A345**, 202 (1980).

[13]J. Delorme et al., Phys. Lett. **89B**, 327 (1980); **91B**, 328 (1980); **99B**, 187 (1981).

[14]Joseph Cohen and J. M. Eisenberg, Phys. Rev. C **29**, 914 (1984).

[15]Joseph Cohen, Phys. Rev. C **30**, 1238 (1984).

[16]M. Cavinato, D. Drechsel, E. Fein, M. Marangoni, and A. M. Saruis, Nucl. Phys. **A423**, 376 (1984).

[17]W. M. Alberico, A. De Pace, and A. Molinari, Phys. Rev. C **31**, 2007 (1985).

[18]H. Toki and W. Weise, Phys. Rev. Lett. **42**, 1034 (1979); H. Toki and W. Weise, Z. Phys. A **292**, 389 (1979).

[19]We notice that in the HO basis, which is utilized in the present

paper, the exact first order $[\hat{\Pi}^{(1)}(q,q';\omega)]_{ll'}$ [left hand side of Eq. (3.1)] can be evaluated analytically. This is done in Appendix B.

[20]P. Schuck, Lecture Notes on the Random Phase Approximation (Trieste, February 1984) (unpublished); U. Stroth, R. W. Hasse, and P. Schuck, in Proceedings of the International Symposium on Highly Excited States and Nuclear Structure (Orsay, 1983).

[21]Joseph Cohen, Phys. Rev. C 30, 1573 (1984).

[22]T. A. Carey et al., Phys. Rev. Lett. 53, 144 (1984).

[23]M. Abramowitz and I. Stegun, Handbook of Mathematical Functions (Dover, New York, 1972), p. 297.